atmosphere

MDPI

Article

Thermal Hazards Evaluation Based on Weight of Evidence Method in the Resource Area of Datong River in Qinghai-Tibetan Plateau

Shengting Wang [1,2,*], Yu Sheng [2], Shuming Jia [1] and Yongzhong Ren [1]

[1] Lanzhou Institute of Technology, Lanzhou 730050, China
[2] State Key Laboratory of Frozen Soil Engineering, Northwest Institute of Eco-Environmental and Resources, Chinese Academy of Sciences, Lanzhou 730000, China
* Correspondence: wangshengting07@163.com

Abstract: With global warming and increasingly frequent human activities in permafrost regions, it is of great significance to accurately and scientifically evaluate the probability and scope of thermal hazards in permafrost regions. Based on remote sensing image interpretation and field survey, the weight of evidence method (WoEM) was used to comprehensively evaluate the risk of thermal hazards in the source area of the Datong River. There were 10 factors, such as ground ice, mean annual ground temperature, mean annual air temperature, and ground soil type etc., selected in the WoEM. The results showed that the thermal hazard occurrences were closely influenced by ground ice, mean annual ground temperature, ground soil type, etc. The thermal hazards mainly occurred in the unstable permafrost with MAGT of –0.5 to –1.5 °C, accounting for 54.72% of the thermal hazards. The distribution area of thermal hazards in ground ice Level I and II accounts for 66.42%. Thermal hazards mainly occur in the soil types of bog soil and sapropel bog soil, accounting for 41.24% and 29.62% of the total thermal hazards area, respectively. Based on the influence factors and WoEM of thermal hazards occurrence, the probability map of thermal hazards occurrence in the source area was obtained. Additionally, the characteristics of the region with a high probability of thermal hazards occurrence and their causes were also comprehensively analyzed.

Keywords: thermal hazards; permafrost; evaluation factors; weight of evidence method; resource area of Datong River

Citation: Wang, S.; Sheng, Y.; Jia, S.; Ren, Y. Thermal Hazards Evaluation Based on Weight of Evidence Method in the Resource Area of Datong River in Qinghai-Tibetan Plateau. *Atmosphere* **2023**, *14*, 885. https://doi.org/10.3390/atmos14050885

Academic Editor: Lin Chen

Received: 15 March 2023
Revised: 17 May 2023
Accepted: 18 May 2023
Published: 18 May 2023

1. Introduction

The Qinghai-Tibet Plateau is a sensitive area of global climate change [1]. Driven by global warming and frequent human activities, the degradation of permafrost, and the associated ground ice melting, is bound to have a great impact on the permafrost environment [2–4]. In particular, permafrost degradation and associated changes in hydrogeological conditions [5–7] have a great impact on the ecological environment [8–12], geological disasters, and permafrost engineering [11–13]. Affected by different landforms, ground soil types, climate, and ground surface conditions [14,15], the thermal state and ice content of permafrost are various [14–16]. In recent years, the permafrost of the Qinghai-Tibet Plateau has been in a state of gradual degradation with the impact of global warming and intensified human activities, such as roads, railways, and mining [17,18]. Such degradation is challenging to permafrost engineering and the stability of existing projects [19,20]. The permafrost degradation is bound to cause a series of thermal hazards, such as thermokarst lakes [21,22], thawing landslides [23,24], and thawing mudflows [25,26]. Especially in areas with high ground ice content and high permafrost temperature, permafrost thaw and its associated impacts on natural and built environments have been identified as a priority issue. The ice content of permafrost is significantly related by landform and lithology [16]. For example, the stratum with fine particles such as silt on the permafrost table, generally

has high ice content [27]. The permafrost temperature is mainly controlled by geographical "three zonality" such as altitude, longitude, and latitude [28], as well as local factors such as climate and surface cover conditions [2,7,8]. Moreover, the above factors interact with each other; the change of a single factor also causes the corresponding change in other factors. Therefore, the assessment of thermal hazards can only be carried out by integrating terrain, environment, climate, permafrost, and other factors. Therefore, it is very necessary for engineers to select a method that can comprehensively and accurately evaluate the thermal hazards in permafrost regions.

Vulnerability assessments of existing and future infrastructure in permafrost regions which include the application of new techniques, including in SAR and geophysical surveys [29,30], as well as regional and community scale hazard assessments [31], are informing adaptation planning. Research conducted at large-scale test facilities, such as that on the Alaska Highway, is supporting assessments of techniques to reduce permafrost thaw [32]. Methodology for geographic assessments of changes in the engineering properties of frozen ground was provided due to observed climatic change [33]. In addition, the popular "unmanned" comprehensive evaluation methods in permafrost regions include the analytic hierarchy process [34], grey correlation analysis method [35], fuzzy comprehensive evaluation [36], catastrophe theory method [37], etc. However, these methods need experts to assign weights or need to manually confirm the importance ranking of factors. Such evaluation results are bound to be significantly affected by human subjective factors. Therefore, this paper tried to adopt a comprehensive evaluation method that is not affected by human subjective factors. At present, there is relatively popular weight evidence of the model (WoEM) [38,39]. The WoEM is mainly a probability method based on probability uncertainty and the Bayesian theorem [38]. In the 1980s, it was first introduced into the prediction and evaluation of mineral resources by mathematical geologists, such as Canada's Agterberg and Bonham-Carter [38,39]. Because it is objective, unaffected by human subjective factors, has a clear structure, and is easy to understand, it has attracted the attention of scholars and experts. With the development of Arc-GIS, the theoretical calculation method has achieved satisfactory results in engineering fields such as mining prediction and evaluation of landslide vulnerability [40,41]. Under the influence of climate change and human activities, permafrost in the source area of Datong River in the Qinghai-Tibetan Plateau is in a degraded state. Through field monitoring and related research, it shows that the mean annual ground temperature (MAGT) gradually increases at a rate of 0.0075 $^{\circ}C \cdot yr^{-1}$ [42], and the area of permafrost has a significant reduction trend [43]. Therefore, the paper attempts to comprehensively evaluate the risk of thermal hazards in the source area of Datong River by the WoEM so as to provide a theoretical basis for the permafrost engineering stability and site selection.

2. Study Area

The source area of Datong River is located in the northeast corner of the Qinghai-Tibet Plateau of China (Figure 1). The altitude is between 3443 m and 5044 m. The lay of the land is NW–SE, with a drainage area of 4573 km^2. The source area is rich in vegetation with a coverage of 63.9%, mainly including alpine meadows and swamp meadows [44]. The lower boundary of the permafrost is about 3650 m, the ice content per unit volume of the shallow layer of the permafrost (3.0–10.0 m) is 0.396 m^3 [45], the mean annual ground temperature (MAGT) of the permafrost is −8.66 to 0 °C, and the active layer thickness (ALT) is 0.9–2.5 m [44,45]. The mean annual air temperature (MAAT) is between −7.08 and 2.26 °C. As the important coal mine base in Qinghai Province, China, some infrastructure was built there, such as Chaimu Railway, roads, and residential houses to serve the local resource development and the residents' living needs.

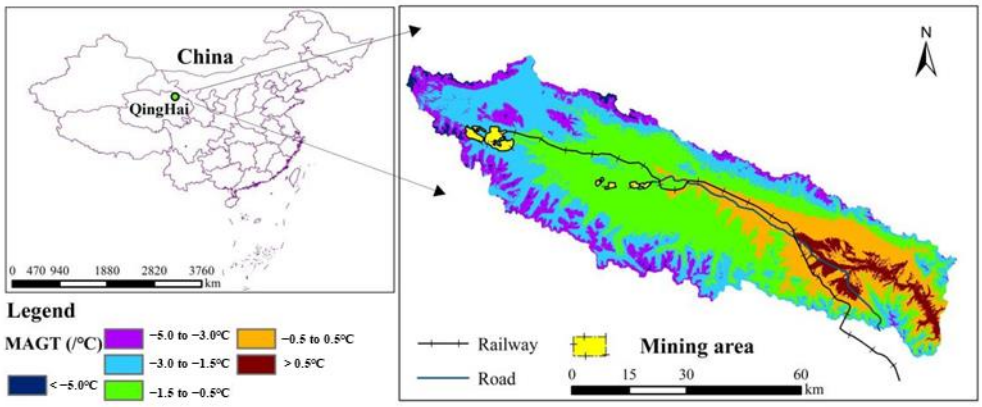

Figure 1. Schematic diagram of study area.

3. Research Methods

The WoEM is based on the Bayesian probability model, which binarizes and calculates the weight of each evidence layer and comprehensively quantifies the evaluation method. The following steps are required according to the calculation sequence.

3.1. Spatial Correlation Calculation (ω^+ and ω^-)

The ω^+ is defined as the influence degree on the evaluation result when a certain disaster occurs in the evidence layer. The ω^- indicates the influence degree on the evaluation results when a certain disaster does not occur in the evidence layer. The correlation judgment can be made by combining ω^+ and ω^-, that is the $\omega^+ > 0$ and $\omega^- < 0$ mean positive correlation between a certain disaster and a certain evidence layer. The $\omega^+ < 0$ and $\omega^- > 0$ mean negative correlation. The 0 indicates no correlation. In order to facilitate comparison and measurement, the concept of contrast is introduced, which is represented by C ($C = \omega^+ - \omega^-$). The contrast value can provide an effective basis for measuring the correlation between disaster points and influence factors. The positive weight (ω^+) and negative weight (ω^-) of each evidence layer are calculated according to Formulas (1) and (2).

$$\omega^+ = \ln \frac{P\{M|F\}}{P\{M|\overline{F}\}} \tag{1}$$

$$\omega^- = \ln \frac{P\{\overline{M}|F\}}{P\{\overline{M}|\overline{F}\}} \tag{2}$$

where $P\{\ |\ \}$ is the Bayesian probability calculation formula.

In order to clarify the above calculation results, it is also necessary to calculate the significance level of the above results (Formulas (3)–(6)).

$$S^2(\omega^+) = \frac{1}{N\{M \cap F\}} + \frac{1}{N\{M \cap \overline{F}\}} \tag{3}$$

$$S^2(\omega^-) = \frac{1}{N\{\overline{M} \cap F\}} + \frac{1}{N\{\overline{M} \cap \overline{F}\}} \tag{4}$$

$$C = S^2(\omega^+) + S^2(\omega^-) \tag{5}$$

$$T(Contrast) = \frac{C}{\sqrt{S^2(\omega^+) + S^2(\omega^-)}} \tag{6}$$

where $S^2(\omega^+)$ and $S^2(\omega^-)$ are the variance of ω^+ and ω^-, *T (Contrast)* is the normalized value of the *C*-value, which can reflect the significance level of the *C*-value (Table 1).

Table 1. T (Contrast) and significant level.

T (Contrast)	0.253	0.542	0.842	1.282	1.645	1.96	2.326	2.576
Significance level	60%	70%	80%	90%	95%	97.5%	99%	99.5%

3.2. Post-Probability Calculation

Combining the weight value calculated in Formulas (1) and (2), the probability of thermal hazards occurrence can be calculated by overlaying the evidence layers. The post-probability needs to be calculated by multiplying the correction factor on the basis of the pre-probability. In the calculating process of spatial correlation weight, it is first necessary to calculate the pre-probability (Formula (7)), which means the probability of disaster occurrence under the condition that any influencing factor or evidence layer is unknown. After the evidence layers are determined, the post-probability can be calculated by Formula (8).

$$P\{F\} = \frac{N\{F\}}{N\{A\}} \tag{7}$$

$$P\{F|M\} = P\{F\} \times \frac{P\{M|F\}}{P\{M\}} \tag{8}$$

where $N\{F\}$ refers to the number of disaster area units, and $N\{A\}$ refers to the number of all area units.

There is not only one evidence layer that affects the thermal hazards. That is, multiply the pre-probability calculation results by the correction factor of each individual layer, and the result is the post-probability. The post-probability can be calculated as Formula (9).

$$P\{F|M_1 \cap M_2 \cap ...M_{...} \cap M_n\} = P\{F\}\frac{P\{M_1|F\}}{P\{M_1\}}\frac{P\{M_2|F\}}{P\{M_2\}}...\frac{P\{M_{...}|F\}}{P\{M_{...}\}}\frac{P\{M_n|F\}}{P\{M_n\}} \tag{9}$$

In order to calculate the weight concisely and clearly, the concept of probability-P is quoted. When the occurrence probability of thermal hazards is greater than that of non-occurrence, the probability-P is greater than 1. When the probability of thermal hazards is less than the probability of non-occurrence, the probability-P is less than 1. Since the premise of the Bayesian probability model is that each layer is independent of the other, the probability model can be simplified as Formulas (10) and (11). Therefore, the above formula can be used to superimpose the area weights obtained from multiple evidence layers. Then it can evaluate the occurrence probability of thermal hazards and generate a comprehensive evaluation map of thermal hazards.

$$P_r = \frac{P}{1-P} \tag{10}$$

$$\ln P_r\left\{F\middle|M_1^{k(1)}M_2^{k(2)}...M_n^{k(n)}\right\} = \ln P_r(F) + \sum_{j=1}^{n}\omega_j^{k(j)} \tag{11}$$

4. Research Data

The permafrost is the product of the earth–atmosphere system and the environment. Climate conditions are the most important boundary conditions of the transition interface between the ground surface and atmosphere, which have profound impacts on the thermal state of permafrost, such as MAAT and MVAT. The mean annual air temperature (MAAT) is the arithmetic mean value of the daily average temperature of each day in a year. The mean variation of air temperature (MVAT) is the range of periodic changes in temperature throughout the year. This is also an important indicator reflecting climate characteristics. Terrain and related conditions profoundly affect the surface heat budget, such as DEM, slope, slope aspect, relief amplitude, and soil type. Relief amplitude refers to the difference

between the maximum elevation and the minimum elevation of all grids within a certain area. It is an important indicator for quantitatively describing landform morphology and dividing landform types. The soil type on the ground surface determines the heat exchange parameters of the ground-air interface. The permafrost-related factors, including MAGT, ATL, and ground ice, are the most direct factors to reflect the permafrost state. The influence degrees of these factors on the thermal hazards occurrence are different. In order to evaluate the thermal hazards more comprehensively and clearly, there were 10 factors selected as the evidence layers for the evaluation, mainly including the terrain and environmental factors, climate factors, and permafrost factors (Figure 2).

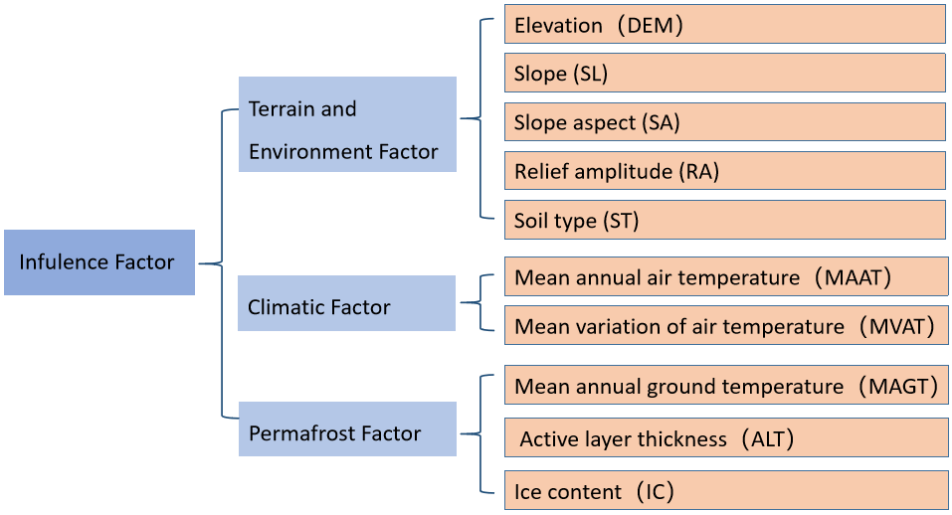

Figure 2. Infulence factors.

4.1. Interpretation of Thermal Hazards Layer

The premise calculation of WoEM is pre-probability. In order to obtain the pre-probability, it is necessary to obtain the general distribution of current thermal hazards. The common types of thermal hazards in the source area of Datong River include thermokarst lakes, thaw slumps, and solifluction. In order to obtain their distribution, the field survey results from 2014 to 2016 and the TM remote sensing image in August 2016 were used to interpret the range of thermal hazards through remote sensing image correction and artificial visual interpretation. The 7, 4, and 3 band synthesis of the TM image can best reflect the real state of the ground surface conditions. The images used for interpretation were synthesized by 7, 4, and 3 bands on the Arc-GIS 10.0 platform. Based on a field survey (location and area) of thermal hazards in the source area of the Datong River from 2014 to 2016 and the corresponding remote sensing images, corresponding relationships were established to interpret the thermal hazards. In this way, the distribution of thermal hazards in the source area was interpreted through manual visual interpretation on the Arc-GIS 10.0 platform (Figure 3). According to the results, the total area of thermal hazards in the source area was 11.45 km^2, with a total number of 399.

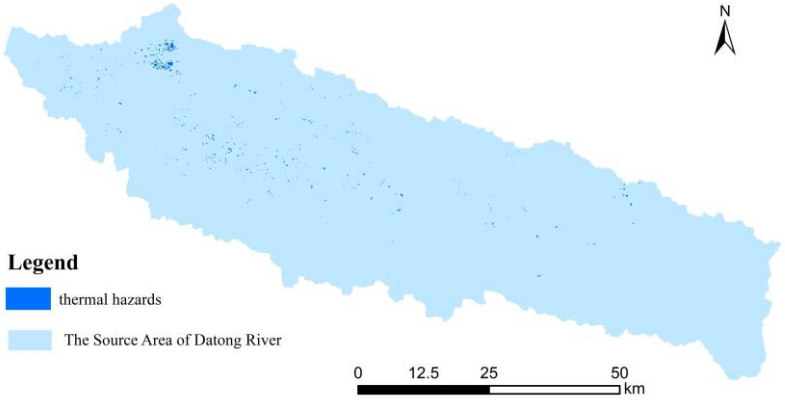

Figure 3. Distribution map of thermal hazards in the source area.

4.2. Terrain and Environmental Factors

According to the importance, elevation (DEM), slope, slope aspect, relief amplitude, and surface soil type were selected as the terrain and environmental factors. In the paper, the natural discontinuity method was used to divide the DEM into six levels (Figure 4a). Under the Arc-GIS platform, the DEM data were used to calculate the slope. The slope data were obtained by the classification criteria adopted in the 1:100,000 topographic mapping specification of China, and the results are shown in Figure 4b. Using the aspect function in the Arc-GIS 10.0 platform, the slope aspect was obtained. Additionally, the slope aspect was graded by a 45-degree interval (flat land represented by −1) (Figure 4c). The different sizes of calculation units in Arc-GIS can lead to different relief amplitude. According to the basic theory of landform development, there exists an optimal analysis unit to achieve a relatively stable maximum elevation difference. The corresponding calculation unit is called the optimal calculation unit. The optimal calculation unit for the relief amplitude in the source area of Datong River was a 10 m × 10 m grid [46]. By spatial analysis, neighborhood analysis in Arc-GIS, the natural discontinuity method was used to divide the relief amplitude into six levels (Figure 4d).

The surface soil type makes the difference in surface thermal conductivity. Based on the 1:100,000 national soil type map provided by the Environmental and Ecological Science Data Center for West China, this paper extracted a total of 14 soil types in the source area, and the soil distribution results are shown in Figure 4e.

4.3. Climate Factors

In the climate factors, the MAAT and mean variation of air temperature (MVAT) were used for evaluation. By the air temperature from 2014 to 2015 in nine simple meteorological monitoring stations of the source area, the MAAT was simulated by multiple regression method (Formula (12)) [47]. The simulation results were divided into six categories by the natural discontinuity method (Figure 4f). The MVAT was also simulated by the multiple regression simulation of temperature data (Formula (13)) [47]. Similarly, the natural discontinuity method was used to divide the MVAT into six categories (Figure 4g).

$$\mathrm{MAAT} = -0.00064E + 10.83085L_a + 4.29784L_o - 843.034, R = 0.90 \quad (12)$$

$$\mathrm{MAVT} = -0.00559E + 1.467929L_a + 0.239812L_o - 46.885, R = 0.88 \quad (13)$$

where E refers to the elevation, L_a refers to the latitude, L_o refers to the longitude, and R refers to the correlation coefficient.

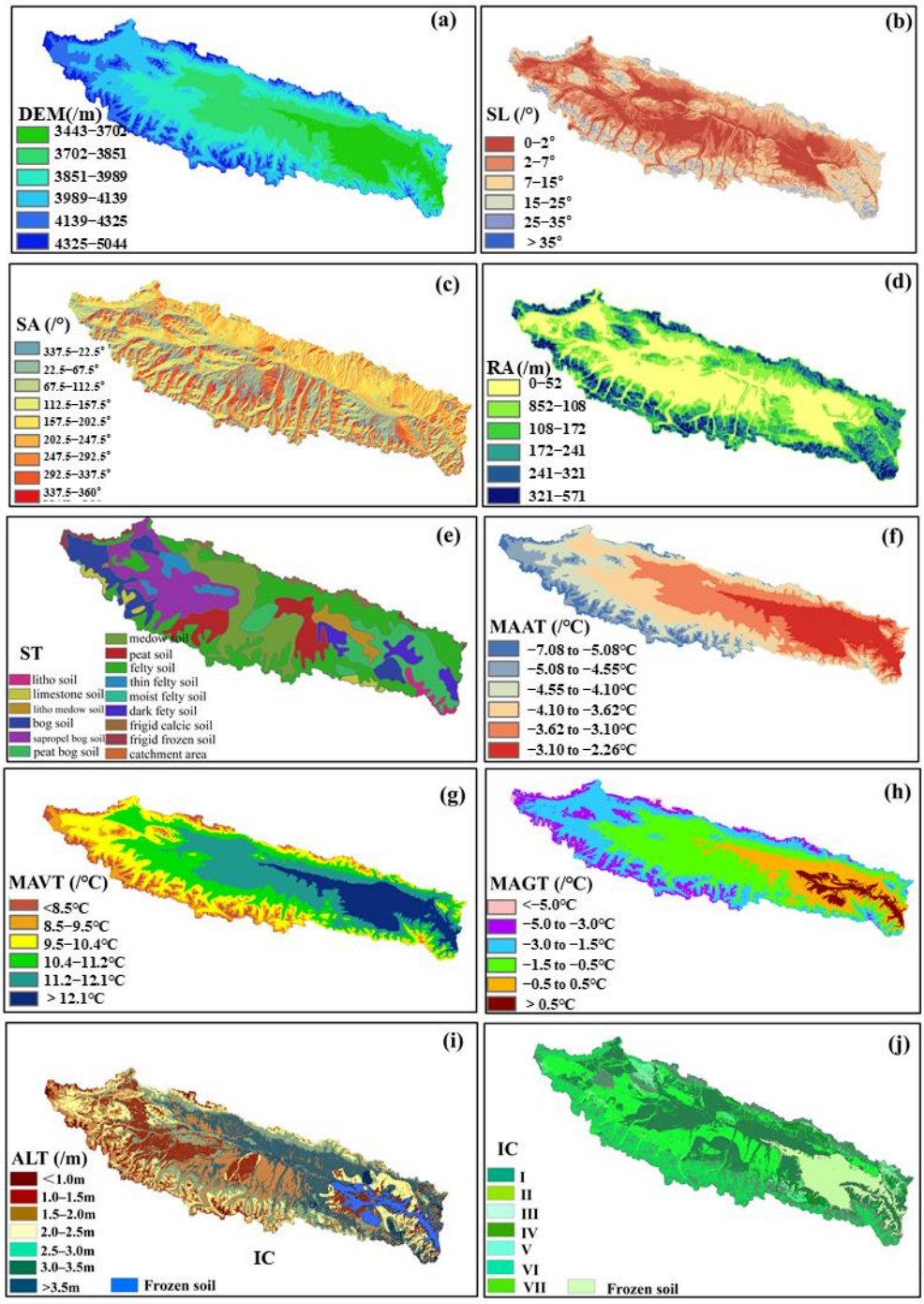

Figure 4. In the grading map of infulence factors (**a**) is elevation (DEM), (**b**) is slope (SL), (**c**) is slope aspect (SA), (**d**) is relief amplitude (RA), (**e**) is surface soil type (ST), (**f**) is MAAT, (**g**) is MVAT, (**h**) is MAGT, (**i**) is ALT, and (**j**) is ground ice (IC).

4.4. Permafrost Factors

Among the relevant factors of permafrost, the MAGT, ALT, and ground ice were selected as the evaluation factors. The MAGT distribution map was obtained by the equivalent elevation method [44] and graded by the "zoning draft" of the permafrost in the Qinghai-Tibet Plateau (Figure 4h) [28]. In order to calculate ATL, based on a large amount of 30 cm ground temperature, the relationships between air temperature and ground temperature at 30 cm with different supergene cover types were established. Then taking 30 cm as the starting depth, the Stefan equation was used to calculate the ATL in the swamp

meadow and alpine meadow areas. For shrub and bare land, the Stefan equation based on the n-factor was used. Finally, the Stefan formulas for calculating the ALT with different supergene cover types were adopted (Figure 4i) [47]. By considering landform types, the corresponding lithological composition, and the measured water content in various landform regions, an approximation demonstrating the existence of many similarities in lithological composition and water content within a unified landform was established during the calculations. Considering the permafrost distribution, extent, and spatial distribution of landform types, the ground ice volume at the depths of 3.0–10.0 m below the ground surface was estimated based on a large number of boreholes from field observations and geological surveys in different types of landforms of the source region. Additionally, the distribution of ground ice in the source region was obtained (Figure 4j) [48].

5. Calculation Results

The evaluation model of thermal hazards includes two aspects: single-factor evaluation and comprehensive evaluation of the selected evaluation factors. Moreover, the prior probability is the basic result of single-factor evaluation. The prior probability results are in Table 2.

Table 2. Prior probability calculation results of thermal hazards.

Total Area (km^2)	Disaster Points	Priori Probability	Average Area (km^2)	Grid Precision (m)	Grid Cell Area (km^2)
4344	399	0.00316	0.03	90 × 90	0.081

5.1. Terrain and Environmental Factors

According to the single-factor calculation results, there was a close relationship between the DEM and thermal hazards. A total of 25.7% and 50.0% of the thermal hazards area are distributed in the elevation range of 3851–3989 m and 3989–4139 m, respectively. Especially in the 3989–4139 m elevation range, the C-value and T (Contrast) are 1.25 and 6.05, respectively, reflecting a high correlation (Table 3). Therefore, the DEM and thermal hazards are closely related. The distribution of slope and thermal hazards is mainly distributed in areas with relatively gentle slopes. According to Table 3, the thermal hazards mostly occur in the plain area with 0–2° slope, accounting for 82.0% of the thermal hazards area. The C-value and T (Contrast) show relatively close relationships. From the slope aspect results, the thermal hazards occur in different directions. The C-value and T (Contrast) in the flat area are relatively large, and the other areas are relatively small (Table 3). Therefore, the relationship between the slope aspect and the thermal hazards is relatively small and can not be listed as an influencing factor. According to Table 3, the thermal hazards are mainly distributed in the relief amplitude range of 0–52 m, with a T (Contrast) of 4.07 and a C-value of 2.64. So, the relationship between the relief amplitude and thermal hazards is closely related (Table 3).

Based on the single-factor results of soil type (Table 3), the correlation between thermal hazards and soil types is relatively high. Thermal hazards mainly occur in the bog soil and sapropel bog soil, accounting for 41.24% and 29.62% of the total thermal hazards area, respectively. The C-value and T (Contrast) are 2.02, 1.00, and 9.29, 3.73, showing a relatively significant correlation.

Table 3. Single factor calculation results of terrain and environmental.

Factor	Category	Zone Area (km^2)	Hazard Area (km^2)	ω^+	ω^-	C	T (C)
DEM (m)	3442–3702	618.32	0.42	−1.49	0.11	−1.61	−0.67
	3702–3851	1068.13	2.36	−0.31	0.08	−0.39	−0.89
	3851–3989	980.91	3.53	0.18	−0.06	0.23	0.78
	3989–4139	1021.91	6.88	0.81	−0.44	1.25	6.05
	4139–4325	632.07	0.57	−1.21	0.11	−1.32	−0.75
	4325–5044	248.50	0.00				
Slope (°)	0–2	1211.38	11.27	1.14	−1.41	2.54	6.15
	2–7	1657.78	1.49	1.21	0.34	−1.55	−2.29
	7–15	947.55	0.71	1.39	0.18	−1.57	−1.11
	15–25	563.89	0.21	2.09	0.12	−2.21	−0.46
	25–35	183.96	0.07	2.01	0.04	−2.05	−0.15
	>35	5.18	0				
Slope aspect (°)	−1	4.93	0.58	3.78	−0.04	3.83	1.95
	337.5–22.5	598.67	2.35	0.27	−0.05	0.31	0.72
	22.5–67.5	660.26	2.32	0.15	−0.03	0.18	0.41
	67.5–112.5	605.07	1.67	−0.09	0.01	−0.10	−0.17
	112.5–157.5	552.03	1.30	−0.25	0.03	−0.27	−0.35
	157.5–202.5	694.36	1.26	−0.51	0.07	−0.58	−0.72
	202.5–247.5	563.73	1.05	−0.48	0.05	−0.53	−0.56
	247.5–292.5	407.44	1.33	0.08	−0.01	0.09	0.12
	292.5–337.5	482.75	1.89	0.27	−0.04	0.30	0.56
Relief amplitude (m)	0–52	1727.08	12.20	0.91	−1.74	2.64	4.07
	52–108	1077.02	0.52	−1.79	0.22	−2.01	−1.04
	108–172	694.26	0.41	−1.58	0.13	−1.71	−0.70
	172–241	603.32	0.38	−1.53	0.11	−1.63	−0.62
	241–321	484.40	0.25	−1.73	0.09	−1.82	−0.45
	321–571	209.19	0				
Soil type	litho soil	60.37	0				
	limestone soil	88.20	0				
	litho medow soil	133.71	0.17	−0.86	0.02	−0.87	−0.15
	bog soil	391.34	5.67	1.58	−0.44	2.02	9.29
	sapropel bog soil	612.12	4.07	0.79	−0.21	1.00	3.73
	peat bog soil	546.99	0.73	−0.82	0.07	−0.90	−0.65
	medow soil	635.80	1.34	−0.36	0.05	−0.41	−0.55
	peat soil	381.86	0.70	−0.51	0.04	−0.54	−0.38
	felty soil	1245.50	0.69	−1.70	0.27	−1.97	−1.36
	thin felty soil	122.63	0.29	−0.25	0.01	−0.26	−0.07
	moist felty soil	3.04	0				
	dark fety soil	190.86	0.10	−1.75	0.04	−1.78	−0.18
	frigid calcic soil	74.06	0				
	frigid frozen soil	57.96	0				
	catchment area	3.04	0				

5.2. Climate Factors

It can be seen from Table 4 that the thermal hazards are mainly distributed in the MAAT range between −4.3 and −1.94 °C. Within the MAAT ranges from −3.51 to −2.74 °C, the distribution area of thermal hazards account for 66.4%, with C-value and T (Contrast) 1.87 and 7.83, showing a relatively significant correlation. Therefore, the MAAT is listed as the evaluation factor. From the calculation results (Table 4), the thermal hazards mainly occur in the MAVT range from 10.4 to 11.2 °C, and the distribution area of thermal hazards in this range accounts for 64.01% of the total thermal hazards area, with C-value and T (Contrast) 1.74 and 7.48, reflecting a relatively close correlation. Therefore, the MAVT was listed as the evaluation factor.

Table 4. Single factor calculation results of climate.

Factor	Category	Zone Area (km^2)	Hazard Area (km^2)	ω^+	ω^-	C	T (C)
MAAT (°C)	<−5.51	239.03	0				
	−5.51 to −4.3	538.55	0.56	−1.07	0.08	−1.16	−0.64
	−4.30 to −3.51	785.10	1.28	−0.62	0.09	−0.71	−0.90
	−3.51 to −2.74	1035.03	9.00	1.06	− 0.81	1.87	7.83
	−2.74 to −1.94	1157.40	2.41	−0.37	0.10	−0.47	−1.11
	>−1.94	796.59	0.51	−1.56	0.16	−1.72	−0.87
MAVT (°C)	<8.5	214.08	0.00				
	8.5–9.5	514.61	0.19	−2.10	0.11	−2.21	−0.42
	9.5–10.4	938.43	1.63	−0.56	0.11	−0.66	−1.07
	10.4–11.2	1089.57	8.80	0.99	−0.75	1.74	7.48
	11.2–12.1	1139.38	2.65	−0.26	0.07	−0.34	−0.86
	>12.1	655.68	0.48	−1.42	0.12	−1.54	−0.74

5.3. Permafrost Factors

MAGT is a direct factor reflecting the thermal state and stability of permafrost. It can be seen from Table 5 that the thermal hazards mainly occur in the unstable permafrost with MAGT from −0.5 to −1.5 °C, accounting for 54.72% of the thermal hazards. Therefore, the MAGT was listed as the evaluation factor. It can be seen from the results (Table 5) that the distribution ranges of ALT are 1.5–2.5 m, 1.0–2.5 m, and 3.0–3.5 m, accounting for 42.77%, 25.86%, and 20.45% of the thermal hazards, and the correlations are high. Therefore, the ATL was listed as an evaluation factor. According to the calculation results (Table 5), there is a high correlation between ground ice and thermal hazards. The thermal hazards are mainly distributed in regions with ground ice Level I and II. In this area, the ground ice is high, and the permafrost is often in an unstable state. From Table 5, the distribution area of thermal hazards (Level I) accounts for 66.42%, and the C-value and T (Contrast) are 1.15 and 4.74, showing a relatively significant correlation.

Table 5. Single factor calculation results of permafrost.

Factor	Category	Zone Area (km^2)	Hazard Area (km^2)	ω^+	ω^-	C	T (C)
MAGT (°C)	>0.5	52.59	0				
	0.5 to −0.5	560.04	0.18	−2.22	0.12	−2.33	−0.43
	−0.5 to −1.5	1382.55	7.53	0.59	−0.43	1.02	4.89
	−1.5 to −3.0	1602.95	5.33	0.10	−0.06	0.15	0.69
	−3.0 to −5.0	736.84	0.63	−1.27	0.13	−1.40	−0.88
	<−5.0	216.61	0.08	−2.08	0.04	−2.12	−0.17
ALT (m)	<1.0	71.38	0.07	−1.15	0.01	−1.16	−0.08
	1.0–1.5	784.43	3.55	0.40	−0.11	0.51	1.71
	1.5–2.5	913.32	5.88	0.75	−0.33	1.09	5.10
	2.5–3.0	308.67	0.52	−0.60	0.03	−0.63	−0.32
	3.0–3.5	1308.72	2.81	−0.35	0.11	−0.46	−1.25
	>3.5	1021.38	0.87	−1.28	0.19	−1.47	−1.27
Ground ice	I	1726.80	9.13	0.55	−0.61	1.15	4.74
	II	1151.49	3.70	0.05	−0.02	0.06	0.22
	III	135.11	0.18	−0.81	0.02	−0.83	−0.15
	IV	157.94	0.20	−0.88	0.02	−0.90	−0.18
	V	77.97	0.17	−0.37	0.01	−0.38	−0.06
	VI	505.14	0.25	−1.82	0.10	−1.92	−0.48
	VII	729.56	0.11	−3.01	0.17	−3.18	−0.35

5.4. Multi-Factors Comprehensive Evaluation

On the basis of the above single-factor evaluation and analysis, the multi-factor evaluation was calculated. Before evaluation, the evaluation factors need to be screened first. The

WoEM often needs to follow the principles before screening the evaluation factors: (1) select the evidence layer with high weight value and close relationship with thermal hazards; (2) each evidence factor should pass the conditional independence test that meets the Bayesian probability model to ensure the thermal hazards are formed by different factors. Try to select two evidence layers with a higher correlation and delete the evidence layer with a lower correlation. It was found that the MAAT and the MAVT were highly correlated during the calculation process, and MAAT was finally selected.

On the basis of the selection principles, the main evaluation factors selected are that the thermal hazards area in the evidence layer accounts for more than 25%, the C-value is more than 1.0, and the T (Contrast) is more than 2.0. The final selected evaluation factors are shown in Table 6.

Table 6. Selection of evaluation factors of WoEM.

Factor Classification	Infulence Factors
Evaluation factors	IC, MAGT, ST, EL, ALT, MAAT, SL, UN
Non-participating factors	SA, MAVT

Based on the selected factors in Table 6, the occurrence probability map of thermal hazards can be obtained. In order to show it more clearly, the natural discontinuity method was used to divide the probability of thermal hazards occurrence into seven levels, and the classification results are shown in Figure 5. According to the probability map of thermal hazards occurrence under different classification levels, the thermal hazards are mainly distributed in the classification of Levels I and VII, which account for 59.6% and 14.2% of the total area (Figure 6). It can be seen that the areas with a high risk of thermal hazards (Level VII) are mainly concentrated in the valley of the source area with plain terrain. From the MAGT and ground ice content, these areas have high MAGT (0 to −1.5 °C) and high ice content. It belongs to unstable permafrost and transitional permafrost. The ATL in these areas is between 1.5 and 2.0 m, surface cover types are mainly swamp meadows with rich moisture content, and the corresponding surface soil type is mainly bog soil. Among them, the area with a higher proportion is Level I, which is mainly distributed in the alpine areas on both sides of the valley, with the characteristics of low MAAT, low MAGT, thin, loose sediments, and low ground ice content.

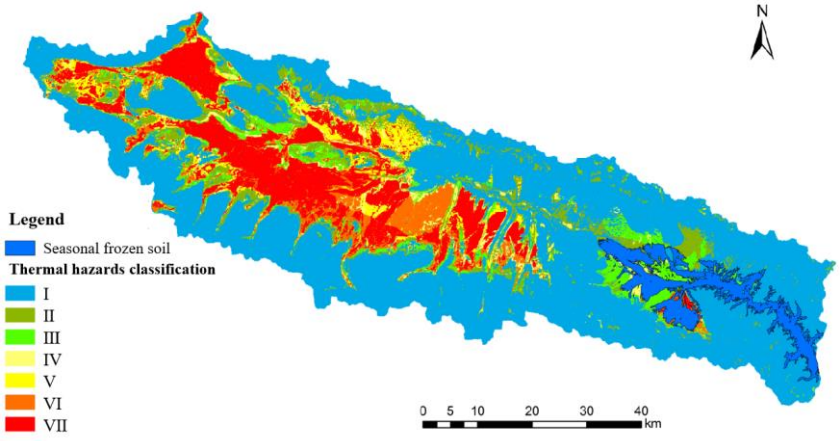

Figure 5. Comprehensive probability evaluation results of thermal hazards.

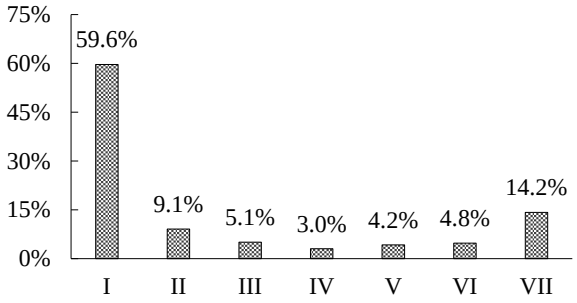

Figure 6. Classification statistics of thermal hazards area.

6. Discussion

The thermal hazards can cause great damage to engineering construction and stability in the future. If engineering projects were built under such geological conditions, it is often necessary to take corresponding measures, which would increase the cost of engineering construction. Therefore, these areas should be avoided as far as possible during the project route and site selection. On the one hand, it can save costs of the project construction; on the other hand, it can guarantee the stability of the project.

The occurrence of thermal hazards is the result of the comprehensive action of many factors. It is particularly important to select comprehensive and reasonable factors to accurately evaluate the probability of its occurrence. From the above analysis, it can be seen that the correlation between ice content, MAGT, and thermal hazards is the highest, especially in terms of ice content. From the distribution of thermal hazards and the ice content, it can be seen that 66.42% of thermal hazards are distributed in areas with high ice content (Level I and II) (Figure 5, Table 5). According to the evaluation results of thermal hazards, although there was a high correlation between MAGT and thermal hazards, there was not a completely positive correlation between them (Figure 5, Table 5). The risk of thermal hazards was the highest with a MAGT from −0.5 to −1.5 °C, and then the risk decreased with the decrease of MAGT. The reason for this characteristic seems to be related to the rich ground ice in these areas. In addition, surface soil type, DEM, ALT, etc., are also closely related to the thermal hazards, and they are important factors affecting the thermal hazards. So, the accuracy of MAGT and ground ice was very important to the results of thermal hazards. However, it is difficult to accurately simulate the MAGT and ground ice of permafrost because the numerical simulation is also affected by many factors. Therefore, the accuracy of its simulation calculation will also have a profound impact on the accurate evaluation of thermal hazards. In particular, the quantitative simulation of ground ice has always been a difficult problem in permafrost research. Although there are some related studies, such as those adopted in this paper [48], their accurate calculation and evaluation need a long time and a large amount of basic data to achieve. Therefore, it is very important to improve the accuracy of these basic data for future research on thermal hazard evaluation.

During the research process of this paper, limited by the scope of the study area, the distribution characteristics of different thermal hazard types, and the precision of remote sensing images, it is not able to establish the accurate interpretation marks of different thermal hazards. Therefore, the different thermal hazard types have not been distinguished in this paper. In the follow-up research, further research can be improved by establishing accurate remote sensing interpretation marks on the basis of expanding the study area and abundant field surveys.

7. Conclusions

The assessment of thermal hazards is affected by many factors. Based on the WoEM and adopting 10 factors, such as ground ice, MAGT, soil type, DEM, ALT, etc., this paper obtains relatively accurate results. From the results, the ground ice, MAGT, soil type, DEM, and ALT are closely related to the thermal hazards occurrence, especially the ground

ice and MAGT. The distribution area of thermal hazards in ground ice (Level I and II) accounted for 66.42%. The thermal hazards mainly occurred in the unstable permafrost with MAGT from −0.5 to −1.5 °C, accounting for 54.72% of the thermal hazards. Thermal hazards mainly occurred in the soil types of bog soil and sapropel bog soil, accounting for 41.24% and 29.62% of the total thermal hazards area, respectively. Therefore, improving the accuracy of these influence factors in the future, especially the ground ice content as a difficulty in permafrost research, would have great significance in improving the accuracy of the thermal hazards evaluation.

Thermal hazards were of great significance to the safety assessment of existing engineering projects and the site selection of future projects. The thermal hazards with high risk distributed in Level VII account for 14.2% of the total area. Moreover, they are mainly concentrated in the valley of the source area with plain terrain, which would be greatly significant to permafrost engineering. In the process of research, restricted by objective factors, this paper did not establish remote sensing interpretation marks for different types of thermal hazards. So the further of research could be improved on the basis of expanding the scope of field investigation and research so as to provide a more accurate basis for engineering safety evaluation.

Author Contributions: Conceptualization, S.W. and Y.R.; Methodology, S.W.; Software, S.W. and S.J.; Validation, Y.R.; Formal analysis, S.W. and S.J.; Resources, Y.S.; Data curation, S.J.; Writing—original draft, S.W.; Supervision, S.W., Y.S. and Y.R.; Project administration, S.W.; Funding acquisition, S.W. All authors have read and agreed to the published version of the manuscript.

Funding: This research was funded by the Gansu Youth Science and Technology Fund Program (grant number 22JR5RA388), the Gansu Province Young Doctor Fund Program (grant number 2022QB-189), and the Youth Science and Technology Innovation Project of Lanzhou Institute of Technology (grant number 19K-010).

Institutional Review Board Statement: Not applicable.

Informed Consent Statement: Not applicable.

Data Availability Statement: All data presented in this paper are available upon request to Shengting Wang (wangshengting07@163.com).

Conflicts of Interest: The authors declare no conflict of interest.

References

1. Ajay, K.; Joginder, S.; Luiz, F. Microbiome Under Changing Climate. In *Chapter 1—Microbes in Thawing Permafrost: Contributions to Climate Change*; Ottoni, J., Vmd, O., Passarini, M., Eds.; Woodhead publishing: Sawston, UK, 2022; pp. 1–28.
2. He, R.; Jin, H.; Luo, D.; Huang, Y.; Ma, F.; Li, X. Changes in the permafrost environment under dual impacts of climate change and human activities in the hola basin, northern da xing'anling mountains, northeast china. *Land Degrad. Dev.* **2022**, *8*, 33. [CrossRef]
3. He, R.; Jin, H.; Ma, F.; Liu, C.; Xiao, D. Recent progress in studying permafrost and cold regions environment in the Hola basin of north Greater Khingan Mountains. *J. Glaciol. Geocryol.* **2015**, *37*, 109–117.
4. Cao, W.; Sheng, Y.; Chou, Y.; Wu, J.; Li, J.; Wang, S. The status evaluation of the permafrost environment along the Chaida'er-Muli Railway in southern Qilian Mountains in northern Qinghai Province, China. *J. Mt. Sci.* **2016**, *13*, 2124–2134. [CrossRef]
5. Cheng, G.; Jin, H. Groundwater in the permafrost regions on the Qinghai-Tibet Plateau and it changes. *Hydrol. Eng. Geol.* **2013**, *40*, 1–11. [CrossRef]
6. Zsoter, E.; Arduini, G.; Prudhomme, C.; Stephens, E.; Cloke, H. Hydrological Impact of the New CMWF Multi-Layer Snow Scheme. *Atmosphere* **2022**, *13*, 727. [CrossRef]
7. Melnikov, A.; Kuznetsov, P. The Influence of Hydrogeological Factors on the Railway Stability in the Areas of Island Permafrost Distribution (by the Example of the Trans-Baikal Railway, Russia). *IOP Conf. Ser. Environ. Earth.* **2021**, *82*, 012063. [CrossRef]
8. Cao, W.; Wan, L.; Zhou, X. A study of the geological environmental of suprapermafrost water in the headwater area of the Yellow River. *Hydrol. Eng. Geol.* **2003**, *6*, 6–10.
9. Wang, G.; Shen, Y.; Cheng, G. Eco-environmental changes and causal analysis in the source regions of the Yellow River. *J. Glaciol. Geocryol.* **2000**, *20*, 200–205.
10. Zhang, S.; Wang, Y.; Zhao, Y. Permafrost degradation and its environmental sequent in the source regions of the Yellow River. *J. Glaciol. Geocryol.* **2004**, *26*, 1–6.
11. Zhang, Y.; Chang, X.; Liang, J. Influence of frozen ground on hydrological process on alpine regions: A case study in an upper reach of the Heihe River. *J. Glaciol. Geocryol.* **2016**, *38*, 1362–1372. [CrossRef]

12. Yao, J.; Yang, Q.; Mao, W. Evaluation of the impacts of climate change and human activities on the hydrological environment in Central Asia. *J. Glaciol. Geocryol.* **2016**, *38*, 222–230. [CrossRef]
13. Chen, L.; Lai, Y.; Fortier, D.; Harris, S.H. Impacts of Snow Cover on the Pattern and Velocity of Air Flow in Air Convection Embankments of Sub-Arctic Regions. *Renew. Energy* **2022**, *199*, 1033–1046. [CrossRef]
14. Penck, W. *Geomorphology Analysis*; Jiang, M., Translator; Department of Geology and Geography: Beijing, China, 1964; pp. 4–65.
15. Vieira, G.; López-Martínez, J.; Serrano, E. Geomorphological observations of permafrost and ground-ice degradation on Deception and Livingston Islands, Maritime Antarctica. In Proceedings of the 9th International Conference on Permafrost, Fairbanks, Alaska, 29 June 2008–3 July 2008; Volume 29, pp. 1839–1844.
16. Wang, S.; Sheng, Y.; Cao, W. Estimation of permafrost ice reserves in the source area of the Yellow River using landform classification. *Adv. Water Sci.* **2017**, *28*, 801–810. [CrossRef]
17. Chen, L.; Voss, C.; Fortier, D.; McKenzie, J. Surface Energy Balance of Sub-Arctic Roads with Varying Snow Regimes and Properties in Permafrost Regions. *Permafr. Periglac.* **2021**, *32*, 681–701. [CrossRef]
18. Cao, W.; Sheng, Y.; Qin, Y.; Wu, L. An application of a new method in permafrost environment assessment of Muli mining area in Qinghai-Tibet Plateau, China. *Environ. Earth.* **2011**, *63*, 609–616. [CrossRef]
19. Wei, M.; Niu, F.; Mu, Y. Basic Research on the Major Permafrost Projects in the QinghaiTibet Plateau. *Adv. Earth Sci.* **2012**, *27*, 1185–1191.
20. Wang, G.; Yu, Q.; You, Y.; Zhang, Z.; Guo, L.; Wang, S. Problems and countermeasures in construction of transmission line projects in permafrost regions. *Sci. Cold Arid. Reg.* **2014**, *6*, 8. [CrossRef]
21. Bouchard, F.; Francus, P.; Pienitz, R.; Laurion, I. Sedimentology and geochemistry of thermokarst ponds in discontinuous permafrost, subarctic Quebec, Canada. *J. Geophys. Res.* **2011**, *116*, 1–14. [CrossRef]
22. Chen, X. Distribution of thermokarst lakers on the Qinghai-Tibet plateau and their regional changes of thermokarst lakers. Doctor's Thesis, Lanzhou University, Lanzhou, China, 2021.
23. Morino, C.; Conway, S.; Saemundsson, T.; Helgason, J.; Argles, T. Mobility of Landslides and Permafrost Degradation Revealed by Molards: Two Case Studies in Northern Iceland. In Proceedings of the 9th International Conference on Geomorphology, New Delhi, India, 6–11 November 2017.
24. Wang, N.; Yao, Y. Characteristics and Mechanism of Landslides in Loess during Freezing and Thawing Periods in Seasonally Frozen Ground Regions. *J. Disaster Prev. Mitig. Eng.* **2008**, *28*, 163–166. [CrossRef]
25. Jin, D.; Niu, F.; Chen, Z.; Ni, W. Landslide hazard from gelifluction in Qinghai-Tibet plateau and stability analysis method. *Coal Geol. Explor.* **2004**, *3*, 49–52.
26. Matsuoka, N. Solifluction and mudflow on a limestone periglacial slope in the Swiss Alps: 14 years of monitoring. *Permafr. Periglac.* **2010**, *21*, 219–240. [CrossRef]
27. Kanevskiy, M.; Shur, Y.; Krzewinski, T. Structure and properties of ice-rich permafrost near Anchorage, Alaska. *Cold Reg. Sci. Technol.* **2013**, *93*, 1–11. [CrossRef]
28. Chen, D.; Wang, S. On the zonation of high-altitude permafrost in China. *Glaciol. Geocryol.* **1982**, *4*, 1–16.
29. Leblanc, A.; Short, N.; Oldenborger, G.; Mathon-Dufour, V.; Allard, M. Geophysical investigation and in Sar mapping of permafrost and ground movement at the Iqaluit airport. In *Cold Regions Engineering 2012, Sustainable Infrastructure Development in a Changing Cold Environment*; Doré, G., Morse, B., Eds.; American Society of Civil Engineers: Reston, VA, USA, 2012; pp. 644–665.
30. Leblanc, A.; Oldenborger, G.; Sladen, W.; Allard, M. Infrastructure and climate warming impacts on ground thermal regime, Iqaluit International Airport, southern Baffin Island, Nunavut. In *Summary of Activities 2014*; Canada-Nunavut Geoscience Office: Iqaluit, NU, Canada, 2015; pp. 119–132.
31. Blais-Steven Kremer, M.; Bonnaventure, P.; Smith, S.; Lewkowicz, A. Active layer detachment slides and retrogressivethaw slumps susceptibility mapping for current and future permafrost distribution, Yukon Alaska Highway Corridor. In Proceedings of the International Association of Engineering Geology Congress, Torino, Italy, 13–19 September 2014; Springer: Berlin/Heidelberg, Germany, 2015; pp. 449–453.
32. Stephani, E.; Fortier, D.; Shur, Y.; Fortier, R.; Dore, G. A geosystems approach to permafrost investigations for engineering applications, an example from a road stabilization experiment, Beaver Creek, Yukon, Canada. *Cold Reg. Sci. Technol.* **2014**, *100*, 20–35. [CrossRef]
33. Streletskiy, D.; Nelson, F. Permafrost, infrastructure, and climate change: A GIS-based landscape approach to geotechnical modelling. *Arct. Antarct. Alp. Res.* **2012**, *44*, 368–380. [CrossRef]
34. Liu, Z.; Yong, Q.; Nie, T.; Qi, Q. Quantitative risk assessment of pipelines in permafrost areas with uncertain analytic hierarchy process and triangular fuzzy number. *J. Chongqing Univ. Technol. (Nat. Sci.)* **2015**, *9*, 137–142. [CrossRef]
35. Wang, L.; Wang, X.; Zhong, H.; Lai, D.; Li, Q. Using hybrid weight grey correlation analysis method to evaluate the environment safety grade of uranium waste rock heap. In Proceedings of the International Conference on Image Analysis & Signal Processing, Melbourne, Australia, 15–18 September 2013; IEEE: Piscataway, NJ, USA, 2013.
36. Chi, Z.; Yang, K.; He, Y.; Yan, X.; Liang, M. Selective preference method of highway route scheme in permafrost regions of qinghai-tibet plateau based on ahp and fuzzy comprehensive evaluation. In Proceedings of the American Society for Composites-37th Technical Conference, Tucson, AZ, USA, 19–21 September 2022.
37. Cao, W.; Sheng, Y.; Qi, J. Assessment of the permafrost environment in the muli mining area in qinghai province based on catastrophe progression method. *J. China Coal Soc.* **2008**, *33*, 881–886.

38. Bonham-Carter, G.; Agterberg, F.; Wright, D. Weights of evidence modelling: A new approach to mapping mineral potential. *Stat. Appl. Earth Sci.* **1989**, *89*, 171–183.
39. Agterberg, F.; Bonham-Carter, G.; Cheng, Q.; Wright, D. Weights of evidence modeling and weighted logistic regression for mineral potential mapping. In *Computers in Geology-25 Years of Progress*; Oxford University Press: Oxford, UK, 1993; pp. 13–32.
40. Zhou, S.; Wang, W.; Chen, G. A combined weight of evidence and logistic regression method for susceptibility mapping of earthquake-induced landslides: A case study of the april 20, 2013 Lushan earthquake, China. *Acta Geol. Sin.* **2016**, *90*, 511–524. [CrossRef]
41. Hong, H.; Ilia, I.; Tsangaratos, P.; Chen, W.; Xu, C. A hybrid fuzzy weight of evidence method in landslide susceptibility analysis on the wuyuan area, China. *Geomorphology* **2017**, *290*, 1–16. [CrossRef]
42. Wang, S.; Sheng, Y.; Wu, J.; Li, J.; Chen, J. The characteristics and changing tendency of permafrost in the source regions of the Datong River, Qilian Mountains. *J. Glaciol. Geocryol.* **2015**, *37*, 27–37.
43. Qi, Y.; Li, S.; Ran, Y.; Wang, H.; Luo, D. Mapping frozen ground in the qilian mountains in 2004–2019 using google earth engine cloud computing. *Remote Sens.* **2021**, *13*, 149. [CrossRef]
44. Li, J.; Sheng, Y.; Chen, J.; Wu, J.; Wang, S. Variations in Permafrost Temperature and Stability of Alpine Meadows in the Source Area of the Datong River, Northeastern Qinghai-Tibet Plateau, China. *Permafr. Periglac.* **2014**, *25*, 307–319. [CrossRef]
45. Wang, S.; Xu, T.; Sheng, Y.; Wang, Y.; Jia, S.; Huang, L. Analysis of Vegetation Coverage Evolution and Degradation under Coal Mine Construction in Permafrost Region. *Atmosphere* **2022**, *13*, 2035. [CrossRef]
46. Wang, S. The Influence of Loose Sediments on the Developing Characteristics of Permafrost in the Source Region of Datong River. Master's Thesis, University of Chinese Academy of Sciences, Beijing, China, 2018.
47. Wang, S. The Spatial Pattern of Permafrost Environment and Engineering Influence Analysis in Source Area of Datong River. Doctor's Thesis, University of Chinese Academy of Sciences, Beijing, China, 2018.
48. Wang, S.; Sheng, Y.; Wu, J.; Li, J.; Huang, L. Based on geomorphic classification to estimate the permafrost ground ice reserves in the source area of the Datong River, Qilian Mountains. *J. Glaciol. Geocryol.* **2020**, *42*, 1186–1194. [CrossRef]